FISEVIER

Contents lists available at ScienceDirect

# Journal of Alloys and Compounds

journal homepage: www.elsevier.com/locate/jalcom



# New layered quaternary $BaCu_6Sn_2As_{4-x}$ and $BaCu_6Sn_2P_{4-x}$ phases: Crystal growth and physical properties



Hanlin Wu<sup>a</sup>, Sheng Li<sup>a</sup>, Xiqu Wang<sup>b</sup>, Sunah Kwon<sup>c</sup>, Wenhao Liu<sup>a</sup>, Gareth A. Ofenstein<sup>a</sup>, Moon J. Kim<sup>c</sup>, Bing Lv<sup>a,c,\*</sup>

- <sup>a</sup> Department of Physics, the University of Texas at Dallas, TX 75080, USA
- <sup>b</sup> Department of Chemistry, University of Houston, Houston, TX 77004, USA
- <sup>c</sup> Department of Materials Science & Engineering, The University of Texas at Dallas, Richardson, TX 75080, USA

#### ARTICLE INFO

Article history: Received 6 April 2021 Received in revised form 22 September 2021 Accepted 23 September 2021 Available online 26 September 2021

Keywords: Intermetallic Quaternary layered compound Cu<sub>2</sub>Sb-type structure Interstitial sites

#### ABSTRACT

We report two new quaternary  $BaCu_6Sn_2As_{4-x}$  and  $BaCu_6Sn_2P_{4-x}$  phases with a new structure type, which are fully characterized by single crystal X-ray diffraction, scanning electron microscopy (SEM), transmission electron microscopy (TEM) and scanning transmission electron microscopy (STEM). These two phases crystallize in tetragonal cell with space group I4/mmm (#139) and Pearson symbol t126. The refined lattice parameters are a=4.164(1) Å, c=24.088(3) Å for  $BaCu_6Sn_2As_{4-x}$ , and a=4.053(2) Å, c=24.08(1) Å for  $BaCu_6Sn_2P_{4-x}$ , respectively. They possess a distinct layered feature composed of  $Cu_6Sn_2Pn_x$  (Pn = P, As) layers sandwiched by the Ba atoms. The Cu-Sn framework of the  $Cu_6Sn_2Pn_x$  layer is closely related to the well-known  $Cu_2Sb$ -type structure, and Pn atoms are found occupying two interstitial sites caused by close packing of Cu and Cu and Cu atoms or capped on the top of square nets formed by Cu atoms. The compounds are also characterized by electrical transport measurements down to 2 K.

© 2021 Elsevier B.V. All rights reserved.

# 1. Introduction

The Cu<sub>2</sub>Sb-type and related structures have been widely studied and are adopted by a huge number of transition metal pnictides with bonding properties ranging from typically ionic over covalent to metallic [1]. The transition metals in these compounds occupy two distinct crystallographic sites: M1 site where metals are tetrahedrally coordinated with pnictide atoms and form planar square nets, and M2 site where metals are coordinated with square pyramids formed by five pnictide atoms and capped with the square nets from M1. Depending on the Wyckoff position distortion/splitting and interstitial-site filling, various prototypic structures including Fe<sub>2</sub>As, UAs<sub>2</sub> (ZrSiS), PbFCl, CeFeSi-type, and the extended HfCuSi<sub>2</sub> and ZrCuSiAs-type structures could be derived [2-5]. The compounds crystallized in these structures display not only fascinating chemistry features, but also a variety of physical properties, including superconductivity, Weyl semimetal, Dirac semimetal, antiferromagnetic order and anomalous Hall effect [6-12]. The paramount example among these phases is the unconventional

E-mail address: blv@utdallas.edu (B. Lv).

superconductivity discovered in the iron pnictide superconductors [6,7,13].

The Cu-based pnictide family, on the other hand, is also rich in both structure diversity and interesting physical or functional applications. The binary Cu<sub>2</sub>Sb and Cu<sub>3</sub>P show promise as an anode material for Li-ion and Na-ion batteries [14-16]. The ternary antiferromagnetic CuMnAs is used as a multi-level memory cell [17]. Structurally, taking ternary Ba-Cu-As system as example, at least five different structures of BaCuAs, BaCu<sub>2</sub>As<sub>2</sub>, BaCu<sub>4</sub>As<sub>2</sub>, BaCu<sub>6</sub>As<sub>2</sub>, and BaCu<sub>8</sub>As<sub>4</sub>, ranging from two-dimensional layers to three-dimensional networks, are known with their analogous phosphides [18–22]. One interesting observation in  $ACu_2Pn_2$  (A = Sr, Ba, and Eu, Pn = P, As and Sb) is that P- and As-based compounds all crystallize in the ThCr<sub>2</sub>Si<sub>2</sub>-type structure, while Sb-based analogs mainly adopt CaBe<sub>2</sub>Ge<sub>2</sub>-type structure or intergrowth of ThCr<sub>2</sub>Si<sub>2</sub> and CaBe<sub>2</sub>Ge<sub>2</sub>type structure [23-26]. Recently, in the course of systematical investigation on the impact of flux for growing copper pnictide single crystals, we have discovered a new β-BaCu<sub>2</sub>As<sub>2</sub> polymorphic phase with unique building sequence [27], which becomes superconducting under high pressure.

The abundant structural diversity in copper pnictides and opportunities for discovery of new materials through flux synthesis have motivated us to explore Cu-based pnictide system and discover new phases with potentially captivate interesting physical

 $<sup>^{\</sup>ast}\,$  Corresponding author at: Department of Physics, the University of Texas at Dallas, TX 75080, USA.

properties. Here, we report two new quaternary  $BaCu_6Sn_2As_{4-x}$  and  $BaCu_6Sn_2P_{4-x}$  phases with a new structure type, which are grown using Sn flux growth method with controlled starting Ba:Cu:Pn ratios. These two compounds adopt the same space group I4/mmm (#139), which are characterized by single crystal X-ray diffraction, SEM, TEM and STEM. The electrical transport measurements on these new compounds indicate overall metallic behaviors from room temperature to 2 K, with electron charge carriers and small positive magnetoresistance under magnetic field of 9 T.

#### 2. Experimental details

#### 2.1. Material synthesis and crystal growth

The starting materials Ba pieces (99.5%), Cu powder (99.99%), Sn shots (99.99%), As lumps (99.999%) and P lumps (99.999%) from Alfa Aesar were stored in Ar-flowed glovebox with a total O<sub>2</sub> and moisture level less than 0.1 ppm. The BaCu<sub>6</sub>Sn<sub>2</sub>As<sub>4-x</sub> crystal is initially discovered as a by-product during crystal growth attempts of BaCu<sub>4</sub>As<sub>2</sub> and BaCu<sub>8</sub>As<sub>4</sub> phases using Sn flux. We observed that this phase also appeared to coexist with β-BaCu<sub>2</sub>As<sub>2</sub> phase under certain specific stoichiometric ratios at low temperature when we previously explore the different synthetic conditions through the different metal flux for the β-BaCu<sub>2</sub>As<sub>2</sub> crystal growth [27]. Given the potential existence of these competing phases, we have carried out series of control experiments with various temperatures and compositions in the starting materials to thoroughly understand the conditions for growing different single crystals and optimize the growth condition for the new phases. The BaCu<sub>6</sub>Sn<sub>2</sub>P<sub>4-x</sub> crystals are grown using the optimized synthesis conditions (discussed later) used for As-analog. We have found out that both the starting materials ratio and synthetic temperature have impacts on the resulting phases during the Sn flux growth. The key results are: 1) when Cu:As ratio is 1:1 (regardless of the Ba amount), we only obtain the Ba<sub>3</sub>Sn<sub>2</sub>As<sub>4</sub> or  $\beta$ -BaCu<sub>2</sub>As<sub>2</sub> phases, where Ba: (Cu,As)  $\geq$  1: 2 ratio vield Ba<sub>3</sub>Sn<sub>2</sub>As<sub>4</sub> crystal and Ba: (Cu,As) < 1: 3 yield β-BaCu<sub>2</sub>As<sub>2</sub> phase in full investigated synthetic temperature range from 800 °C to 1100 °C; 2) when the ratio of Cu:As is larger than 1:1 (e.g. Cu:As= 2:1, 3:1 4:1, 6:1 and 7:1 in our experiments) and under the high synthetic temperature range from 900 °C to 1100 °C, only BaCu<sub>6</sub>Sn<sub>2</sub>As<sub>4-x</sub> single crystals are produced. Higher synthetic temperature intends to produce bigger crystals; 3) when the ratio of Cu:As is larger than 1:1, but the highest synthetic temperature is below 800 °C, both BaCu<sub>6</sub>Sn<sub>2</sub>As<sub>4-x</sub> and β-Ba-Cu<sub>2</sub>As<sub>2</sub> single crystals were formed. The optimized synthetic condition for the growth of large size BaCu<sub>6</sub>Sn<sub>2</sub>As<sub>4-x</sub> and BaCu<sub>6</sub>Sn<sub>2</sub>P<sub>4-x</sub> single crystals, therefore, is chosen using Ba:Cu:As (P):Sn with a molar ratio of 1:8:4:30.

The related starting materials are weighted accordingly and loaded into an alumina crucible inside the glovebox. The alumina crucible container with the starting materials is then flame-sealed in an evacuated quartz tube. The quartz tube assembly with the container is then heated from room temperature up to 1100 °C in 20 h, stayed at 1100 °C for 24 h and then slowly cooled to 500 °C at a rate of 3 °C/h. Silver plate-like crystals with a typical size of  $3\times2\times0.1~\text{mm}^3$  were obtained by decanting the flux with a centrifuge at 500 °C using quartz wool as a filter.

#### 2.2. Characterization

X-Ray Diffraction: Single-crystal X-ray diffraction was performed using a Bruker SMART diffractometer equipped with an Apex II area detector, and an Oxford Cryosystems 700 Series temperature controller. A hemisphere of frames was measured using a narrow-frame method with a scan width of  $0.30^{\circ}$  in  $\omega$  and an exposure time of 30 sframe with Mo K<sub>\alpha</sub> radiation. The collected dataset was integrated using the Bruker Apex-II program, with the intensities corrected for the Lorentz factor, polarization, air absorption, and absorption due to variation in the path length through the detector faceplate. The data was scaled, and absorption correction was applied using SADABS [28]. A starting model was obtained using the intrinsic method in SHELXT [29], and atomic sites were refined anisotropically using SHELXL2018. Crystallographic parameters and refinement details for BaCu<sub>6</sub>Sn<sub>2</sub>As<sub>4-x</sub> and BaCu<sub>6</sub>Sn<sub>2</sub>P<sub>4-x</sub> are provided in Table 1. Atomic coordinates, equivalent anisotropic displacement parameters, occupancies and some selected interatomic distances are included in Tables 2 and 3. For the BaCu<sub>6</sub>Sn<sub>2</sub>As<sub>4-x</sub>, the partial occupancy of As2 is fixed to the elemental analysis values obtained from SEM-EDX results. For BaCu<sub>6</sub>Sn<sub>2</sub>P<sub>4-x</sub>, fixed occupancy of P2 position close to SEM-EDX results always goes to non-positive-definite therefore we present our results where P2 position is refined freely. It is noted that chemical analysis uncertainty is typically higher for light elements from SEM-EDX. Powder X-ray diffraction (XRD) was performed using a Rigaku Smartlab diffractometer with Cu K<sub>\alpha</sub> radiation to investigate the preferred orientation of the single crystals.

SEM: The composition and mapping data was collected by SEM energy-dispersive X-ray spectroscopy (SEM-EDX) using Zeiss EVO LS 15 SEM with accelerating voltage of 20 keV. The data was collected on several crystals with at least five measured points for each crystal to determine the composition.

TEM and STEM: Atomic resolution high angle annular dark field scanning transmission electron microscopy (HAADF-STEM) images and high-resolution TEM (HRTEM), selected area electron diffraction (SAED) were acquired using an aberration-corrected JEM-ARM200F

**Table 1**Crystallographic details for BaCu<sub>6</sub>Sn<sub>2</sub>As<sub>4-x</sub> and BaCu<sub>6</sub>Sn<sub>2</sub>P<sub>4-x</sub>.

Formula	BaCu <sub>6</sub> Sn <sub>2</sub> As <sub>2,46</sub>	$BaCu_6Sn_2P_{2.72}$	
Temperature	295(2) K	295(2) K	
Wavelength	0.71073 Å	0.71073 Å	
Space group	I4/mmm (No.139)	I4/mmm (No.139)	
Unit cell dimensions	a = b = 4.164(1)Å,	a = b = 4.053(2)Å, $c = 24.08(2)$ Å	
	c = 24.088(3)  Å		
Volume	417.60 (11) Å <sup>3</sup>	395.5 (5) Å <sup>3</sup>	
Z	2	2	
Absorption coefficient	35.840 mm <sup>-1</sup>	27.337 mm <sup>-1</sup>	
F(000)	822	742	
Crystal size	$0.11 \times 0.10 \times 0.01 \text{ mm}^3$	$0.31 \times 0.10 \times 0.01 \text{ mm}^3$	
Theta range for data collection	3.38-28.26°	3.38-28.31°	
Reflections collected	1413	1363	
Independent reflections	198 [R <sub>int</sub> = 0.0567]	182 [R <sub>int</sub> = 0.0490]	
Data/Restraint/parameter	198/0/18	182/0/20	
Goodness-of-fit on F <sup>2</sup>	1.223	1.136	
Final R indices[I > 2sigma(I)]	R1 = 0.0382, $wR2 = 0.1119$	R1 = 0.0232, $wR2 = 0.0558$	
R indices (all data)	R1 = 0.0389, $wR2 = 0.1126$	R1 = 0.0236, $wR2 = 0.0563$	
Largest diff. peak and hole	1.673/- 1.326	1.435/- 1.082	

BaCu <sub>6</sub> Sn <sub>2</sub> As <sub>4-x</sub>										
Atom	Wyck.	Symm.	X	y	Z	Occ.	$U_{eq}^{a}(Å^{2})$			
Ba1	2a	4/mmm	1/2	1/2	1/2	1	0.0229(5)			
Cu1	8 g	2mm.	0	1/2	0.37553(8)	1	0.0345(6)			
Cu2	4e	4mm	0	0	0.31406(10)	1	0.0286(7)			
Sn1	4e	4mm	0	0	0.20289(7)	1	0.0571(8)			
As1	4e	4mm	0	0	0.42623(8)	1	0.0223(6)			
As2	4d	-4m2	1/2	0	1/4	0.23	0.0139(15)			
$BaCu_6Sn_2P_{4-x}$										
Atom	Wyck.	Symm.	x	у	z	Occ.	$U_{eq}^{a}(Å^{2})$			
Ba1	2a	4/mmm	1/2	1/2	1/2	1	0.0101(3)			
Cu1	8 g	2mm.	0	1/2	0.37833(4)	1	0.0152(3)			
Cu2	4e	4mm	0	0	0.31510(5)	1	0.0121(4)			
Sn1	4e	4mm	0	0	0.20569(3)	1	0.0242(3)			
P1	4e	4mm	0	0	0.42421(10)	1	0.0081(5)			
P2	4d	-4m2	1/2	0	1/4	0.36(2)	0.027(3)			

 $<sup>^{\</sup>rm a}~U_{\rm eq}$  is defined as one-third of the trace of the orthogonalized  $U_{\rm ij}$  tensor.

Table 3 Selected atomic distances of BaCu $_6$ Sn $_2$ As $_{4-x}$  and BaCu $_6$ Sn $_2$ P4 $_{-x}$ .

BaCu <sub>6</sub> Sn <sub>2</sub> As <sub>4-x</sub>			BaCu <sub>6</sub> Sn <sub>2</sub> P <sub>4</sub>	BaCu <sub>6</sub> Sn <sub>2</sub> P <sub>4-x</sub>		
Sn1-Cu1	(×4)	2.811(2)	Sn1-Cu1	(×4)	2.864(2)	
Sn1-Cu2	(×1)	2.678(3)	Sn1-Cu2	(×1)	2.635(2)	
Sn1-Cu2	(×4)	2.972(1)	Sn1-Cu2	(×4)	2.909(2)	
Sn1-As2	(×4)	2.371(1)	Sn1-P2	(×4)	2.290(2)	
Cu1-Cu1	(×4)	2.944(1)	Cu1-Cu1	(×4)	2.866(2)	
Cu1-Cu2	(×2)	2.555(2)	Cu1-Cu2	(×2)	2.535(2)	
Cu1-As1	(×2)	2.414(2)	Cu1-P1	(×2)	2.308(2)	
Cu2-As1	(×1)	2.702(3)	Cu2-P1	(×1)	2.628(3)	
Cu2-As2	(×4)	2.591(2)	Cu2-P2	(×4)	2.562(2)	

(JEOL USA Inc.) operated at 200 kV. SAED simulation was performed by JEMS software. TEM lamellas were prepared using an FEI Nova 200 dual-beam focused ion beam system (FIB, FEI Inc.) by the lift-out method.

Electrical Transport Studies: Electrical resistivity  $\rho(T, H)$  using four probe configuration, and Hall resistivity measurements using five probe configuration, were measured down to 2 K and up to 9 T magnetic field in a Quantum Design Physical Property Measurement System (PPMS).

#### 3. Results and discussion

# 3.1. Structural Description

The BaCu<sub>6</sub>Sn<sub>2</sub>As<sub>4-x</sub> and BaCu<sub>6</sub>Sn<sub>2</sub>P<sub>4-x</sub> are isostructural with each other, which crystallize in a new structure type (**t126**) and tetragonal space group *I4/mmm* (#139). The refined lattice parameters are a=b=4.164(1) Å, c=24.088(3) Å for BaCu<sub>6</sub>Sn<sub>2</sub>As<sub>4-x</sub> and a=b=4.053(2) Å, c=24.08(1) Å, BaCu<sub>6</sub>Sn<sub>2</sub>P<sub>4-x</sub>, respectively, where no significant change of lattice c is observed from As-analog to P-analog. To the best of our knowledge, these two samples are the first quaternary compounds discovered in Ba-Cu-Sn-Pn system. The structures are tightly related to Cu<sub>2</sub>Sb-type building motifs. Fig. 1 shows our rational analysis of this distinct structure, where the separation is only formal since the shortest bond distances of Cu1-Pn1, Cu2-Pn2, Sn-Pn2 are 2.414(2) Å, 2.591(2) Å, 2.371(1) Å for BaCu<sub>6</sub>Sn<sub>2</sub>As<sub>4-x</sub> and 2.308(2) Å, 2.562(2) Å, 2.290(2) Å for BaCu<sub>6</sub>Sn<sub>2</sub>P<sub>4-x</sub>, respectively.

Like the  $Cu_2Sb$ -type structure, there are two distinct Cu crystal-lographic sites in this structure, where  $Cu_1$  atoms at the 8g site form a square planar net, and  $Cu_2$  atoms at the 4e site are coordinated with five neighboring tin atoms rather than pnictide atoms (Fig. 1a). The  $Cu_3S_5$  square pyramid by  $Cu_2$  atoms is capped with the planar square net by  $Cu_1$  atoms, and forms a  $[Cu_6Sn_2]$  slab. The  $Cu_1$ - $Cu_2$  distances range from 2.535(2) to 2.555(2) Å, suggesting effective bonding between two different types of Cu atoms. Two  $[Cu_6Sn_2]$ 

slabs, are arranged centrosymmetrically in the unit cell together with Ba atoms, and form a  $[Ba_2Cu_{12}Sn_4]$  =  $BaCu_6Sn_2$  layered framework. The Cu-Sn distances of 2.635(2)-2.972(1) Å, are comparable to those found in the intermetallic compounds, which are 2.688-2.757 Å for  $Cu_3Sn$  [30], 2.631-2.863 Å for  $Cu_6Sn_5$  [31], 2.644-2.792 Å for  $BaCuSn_2$  [32] and 2.674 Å for DyCuSn [33].

Pn atoms reside in the layered framework, as shown in Fig. 1b. Pn1 atoms are capped above the center of the square net formed by Cu1 atoms, and form PnCu<sub>4</sub> square pyramids with the Cu1-As1 distance of 2.414(2) Å in BaCu<sub>6</sub>Sn<sub>2</sub>As<sub>4-x</sub> and Cu1-P1 distance of 2.308(2) Å in BaCu<sub>6</sub>Sn<sub>2</sub>P<sub>4-x</sub>. Each Pn1 atom is surrounded by four Ba atoms and four Cu1 atoms, which forms a highly distorted square antiprism shown in Fig. 1b. The Ba1-Pn1 distances are above 3 Å [3.439(2) Å for Ba1-As1 and 3.398(2) Å for Ba1-P1], suggesting no effective bonding interaction between these two atoms. The Pn2 atoms, on the other hand, are in the interstitial sites tetrahedrally surrounded by four Sn1 atoms and four Cu2 atoms. The Pn1 atoms in the large square antiprism are fully occupied due to the relatively larger distances between Ba and Cu1 atoms [3.650(2) Å for Ba- $Cu_6Sn_2As_{4-x}$  and 3.391(2) Å for  $BaCu_6Sn_2P_{4-x}$ ]. For Pn2 atoms, the tetrahedral interstitial sites are relatively small due to the relatively short Cu2-Sn distances [2.678(3)Å for BaCu<sub>6</sub>Sn<sub>2</sub>As<sub>4-x</sub> and 2.635(2) Å for BaCu<sub>6</sub>Sn<sub>2</sub>P<sub>4-x</sub>]. Therefore, Pn2 atoms have rather low occupancies [0.33(1) for As2 and 0.36(2) for P2], which result in a formal Ba-Cu<sub>6</sub>Sn<sub>2</sub>As<sub>2,46</sub> and BaCu<sub>6</sub>Sn<sub>2</sub>P<sub>2,72</sub> from single crystal X-ray refinements.

All the Pn-Cu bonding distances [2.414(2)-2.702(3) Å for  $BaCu_6Sn_2As_{2.46}$  and 2.308(2)-2.628(3) Å for  $BaCu_6Sn_2P_{2.72}$ ] are comparable to those of reported Cu-related pnictides such as  $BaCu_2As_2$ ,  $BaCu_6As_2$ ,  $BaCu_8Pn_4$ , and BaCuP [18,21,22,27]. The close packing of Pn2 atoms at the tetrahedral interstitial site has significantly impacted Sn1-Pn2 interaction. The bonding distances for Sn1-Pn2 [2.371(1) Å for Sn1-As2, 2.290(2) Å for Sn1-P2] are much shorter than the Sn-Pn distances in known intermetallic compounds, e.g. 2.461 Å in SrSnP [34], 2.442–2.676 Å in Ba<sub>3</sub>Sn<sub>2</sub>P<sub>4</sub> [35], or 2.572–2.639 Å in Ca<sub>5</sub>Sn<sub>2</sub>As<sub>6</sub> [36], 2.587–2.690 Å in Ba<sub>3</sub>Sn<sub>2</sub>As<sub>4</sub> [37]. We have also carried out experiments with intention to increase Pn2 occupancies by increasing As and P amount in the starting materials following similar synthesis procedures described in the experimental section. The crystals synthesized from different batches are all refined with nearly the same lattice parameters and Pn2 occupancies within measured errors from single crystal X-ray refinements.

The occupancy of guest atoms at the tetrahedral interstitial sites in Cu<sub>2</sub>Sb-related structures or compounds with Cu<sub>2</sub>Sb-type building motifs, in fact, are very rare, as typically the neighboring metalmetal distance forming the tetrahedral sites are relatively shorter, which will be difficult to accommodate any excess guest atoms without a very large distortion. To further validate the structures of the crystals, we carry out the HRTEM and atomic resolution HAADF-STEM studies. As both phases are isostructural, we only select BaCu<sub>6</sub>Sn<sub>2</sub>As<sub>2,46</sub> crystal for these studies. Because in principle, the larger As atoms, as guest atoms, should be more difficult to occupy the interstitial sites. HRTEM and HAADF-STEM images are created, while SAED and STEM imaging are carried out along the [100] zone axis. All SAED simulations are conducted using constructed models that are built based on single crystal diffraction results. Fig. 2a shows the measured SAED pattern of BaCu<sub>6</sub>Sn<sub>2</sub>As<sub>2,46</sub>, indicating good crystallinity of our sample. It is well consistent with the simulated pattern (Fig. 2b), suggesting the constructed models accurately represent the actual structure of BaCu<sub>6</sub>Sn<sub>2</sub>As<sub>2,46</sub>. Fig. 2c is the HADDF-STEM image taken from BaCu<sub>6</sub>Sn<sub>2</sub>As<sub>2.46</sub> single crystal along the [001] zone axis. Obtained STEM images are filtered to enhance contrast by removing noise. The uniformity in this image indicates that the lattice contains no extended defects. The existence of each element is additionally confirmed by STEM and EDS. The length of the unit cell is estimated to be 24.1 Å, which is consistent with the result

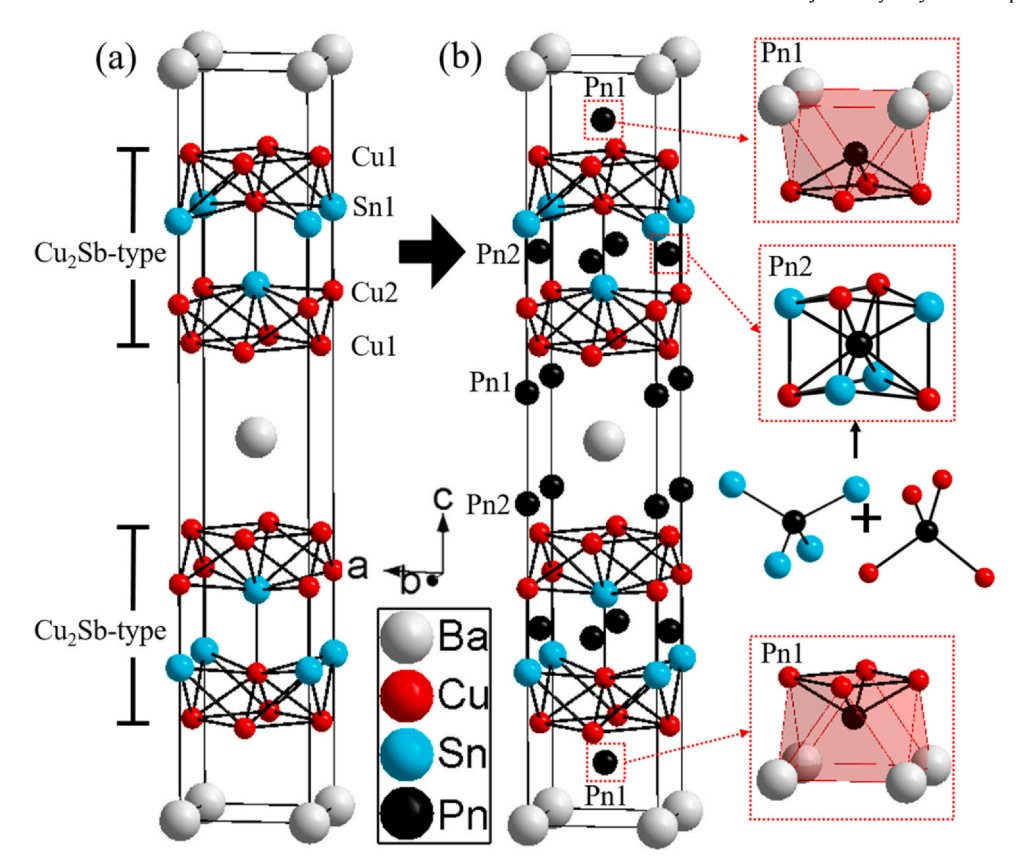


Fig. 1. Crystal structure of BaCu<sub>6</sub>Sn<sub>2</sub>Pn<sub>4-x</sub> (Pn=As and P) based on single crystal X-ray diffraction. (a) Cu<sub>2</sub>Sb-type building motif formed by Cu<sub>1</sub>, Cu<sub>2</sub> and Sn atoms with sandwiched Ba atoms. (b) Crystal structure with highlighted environment of Pn<sub>1</sub> and Pn<sub>2</sub> atoms. Pn<sub>1</sub> atoms form the square antiprism with four Ba atoms and four Cu<sub>1</sub> atoms. Pn<sub>2</sub> atoms are tetrahedrally surrounded by four Sn atoms and four Cu<sub>2</sub> atoms.

from single crystal diffraction. For better comparison, an enlarged STEM image is shown in Fig. 2d. In these Z-contrast HAADF images, each atom can be distinguished by brightness and size. Ba atoms are clearly recognized as bright dots, Sn atoms are less bright than Ba atoms but are brighter than Cu atoms and As atoms, while Cu atoms are less bright than As atoms. Due to low occupancy, As2 atoms are not as bright as other atoms, but we can still observe blurry spots between Sn atoms and Cu atoms. The constructed model is overlapped with image to confirm its consistency. The crystal structure we observed is clearly consistent with results from single crystal X-ray diffraction and SAED pattern. These results confirm low occupancy of guest As atoms at the tetrahedral interstitial sites and uniqueness of the structures of these two quaternary phases.

# 3.2. Characterization

The grown crystals are typically ~ 2 mm in size and with shiny flat surface (inset of Fig. 3a), which is large enough for us to carry out meaningful physical measurements. The flat surface is expected to be along ab plane as evidenced by the preferred orientation along c-axis in powder X-ray diffraction patterns with indexed indices (Fig. 3a). The SEM-EDX analysis on the flat crystals confirmed the existence of the elements with chemical ratio of Ba:Cu:Sn:As = 1.01(3):6.17(8):2.01(3):2.46(9) for BaCu\_6Sn\_2As\_{4-x} single crystals, and Ba:Cu:Sn:P = 1.06(1):5.98(2):2.13(3):2.37(3) for BaCu\_6Sn\_2P\_{4-x} single crystals. The slight composition discrepancy of P element between SEM and X-ray single crystal refinement might be due to the higher uncertainty of light elements in the EDX chemical analysis as noted before. The SEM-EDX mapping results are shown in Fig. 3b suggesting the homogeneous distribution of the elements across a large area of  $1.5\times 1~\mathrm{mm}^2$  size BaCu\_6Sn\_2As\_{4-x} crystal.

Fig. 4a shows temperature-dependent in-plane electrical resistivity of  $BaCu_6Sn_2As_{2.46}$  and  $BaCu_6Sn_2P_{2.72}$  single crystals. Typical metallic behaviors are observed over whole measured temperature range from 2 K to 300 K. The room temperature resistivity is  $177.5\,\mu\Omega$  cm for  $BaCu_6Sn_2As_{2.46}$  and  $212.0\,\mu\Omega$  cm for  $BaCu_6Sn_2P_{2.72}$ , which are comparable to typical Cu-rich intermetallic compound such as Cu\_3Sn of  $8.8\,\mu\Omega$  cm, Cu\_6Sn\_5 of  $17.5\,\mu\Omega$  cm and Cu\_2Sb of  $16\,\mu\Omega$  cm [38,39]. The overall residual resistivity ratio (RRR) is small, 1.73 for  $BaCu_6Sn_2As_{2.46}$  and 2.14 for  $BaCu_6Sn_2P_{2.72}$ , which are likely due to the partial occupancies (i.e., defects) caused by the pnictide atoms.

The temperature dependent electrical resistivity appears to follow conventional Bloch-Grüneisen (BG) formula:

$$\rho(T) = \rho_0 + \rho_{BG} = \rho_0 + 4A \left(\frac{T}{\Theta_D}\right)^5 \times \int_0^{\Theta_D/T} \frac{x^5 dx}{(e^x - 1)(1 - e^{-x})}$$

where  $\rho_0$  is the residual resistivity due to scattering of conduction electrons on lattice impurities,  $\Theta_D$  is the Debye temperature obtained from a fit of experimental resistivity data by the BG theory, and A is a coefficient representing scattering strength of electrons with acoustic phonons. The fitting results are quite satisfactory, suggesting temperature dependent resistivity could be well explained through the scattering of conduction electrons by longitudinal acoustic lattice vibrations. The values we obtained through fitting are  $\rho_0$ = 104.20(1)  $\mu\Omega$  cm, A = 39.9(1)  $\mu\Omega$  cm and  $\Theta_D$ = 159.8(5) K for BaCu<sub>6</sub>Sn<sub>2</sub>As<sub>2.46</sub>, and  $\rho_0$ = 98.74(8)  $\mu\Omega$  cm, A= 28.5(7)  $\mu\Omega$  cm, and  $\Theta_D$ = 74.8(19) K for BaCu<sub>6</sub>Sn<sub>2</sub>P<sub>2.72</sub>, respectively.

A small magnetoresistance [MR= $(\rho_{xx}(B)-\rho_{xx}(0))/\rho_{xx}(0)]$ , ~2.6% for BaCu<sub>6</sub>Sn<sub>2</sub>As<sub>2.46</sub> and 1.5% for BaCu<sub>6</sub>Sn<sub>2</sub>P<sub>2.72</sub> at 2 K and under 9 T magnetic field, is observed shown in the inset of Fig. 4a. These values fall into the conventional weak magnetoresistance values (~2%)

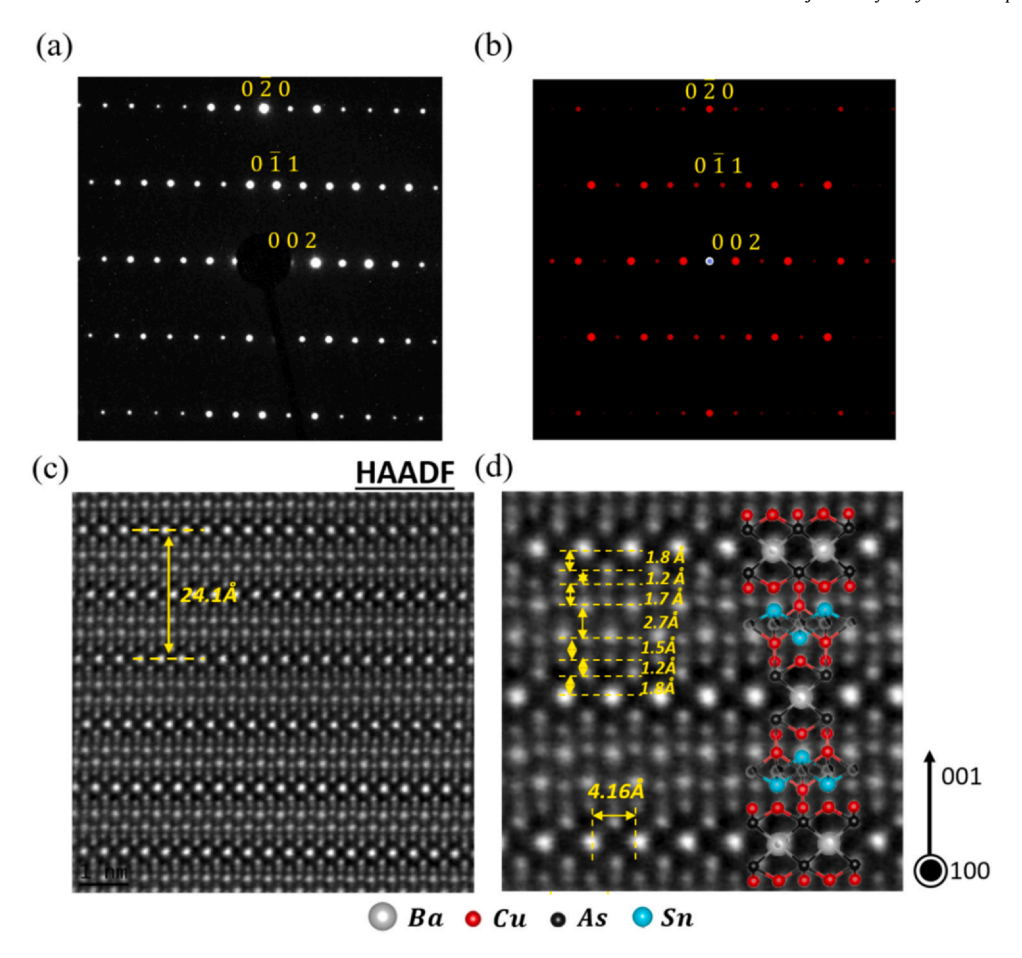


Fig. 2. (a) Measured SAED pattern; (b) Simulated SAED pattern; (c) STEM image of BaCu<sub>6</sub>Sn<sub>2</sub>As<sub>2,46</sub> single crystal with estimated length of unit cell; (d) Enlarged STEM image with estimated length of crystal and simulated crystal model for better comparison.

observed in the normal nonmagnetic metals. This type of magnetoresistance in metals or semimetals is typically characterized with quadratic field dependence in low fields. We have fitted field-dependent magnetoresistance data of our samples by empirical formula  $\Delta \rho(H) = a H^{\delta}$ , and obtained  $\delta$  value of 1.64(1) for BaCu<sub>6</sub>Sn<sub>2</sub>As<sub>4-x</sub> and 1.67(1) for BaCu<sub>6</sub>Sn<sub>2</sub>P<sub>4-x</sub>, which are close to the expected values. These results are consistent with magnetic susceptibilities measurements where a temperature-independent Pauli-paramagnetic behavior is observed for both compounds.

To further obtain type of charge carriers and carrier concentrations, we have measured field-dependent Hall resistivity at 2 K for both BaCu<sub>6</sub>Sn<sub>2</sub>As<sub>2.46</sub> and BaCu<sub>6</sub>Sn<sub>2</sub>P<sub>2.72</sub> single crystals as shown in Fig. 4b. The Hall resistivity shows linearly dependent behavior as a function of the magnetic field. Both slopes are negative, indicating charge carriers are dominantly electrons near the Fermi surface. Through simple calculation using  $n = \frac{B}{e \rho_{xy}}$ , the carrier concentration is estimated to be  $1.4 \times 10^{22}$  cm<sup>-3</sup> for BaCu<sub>6</sub>Sn<sub>2</sub>As<sub>2.46</sub> and  $4.5 \times 10^{22}$ 

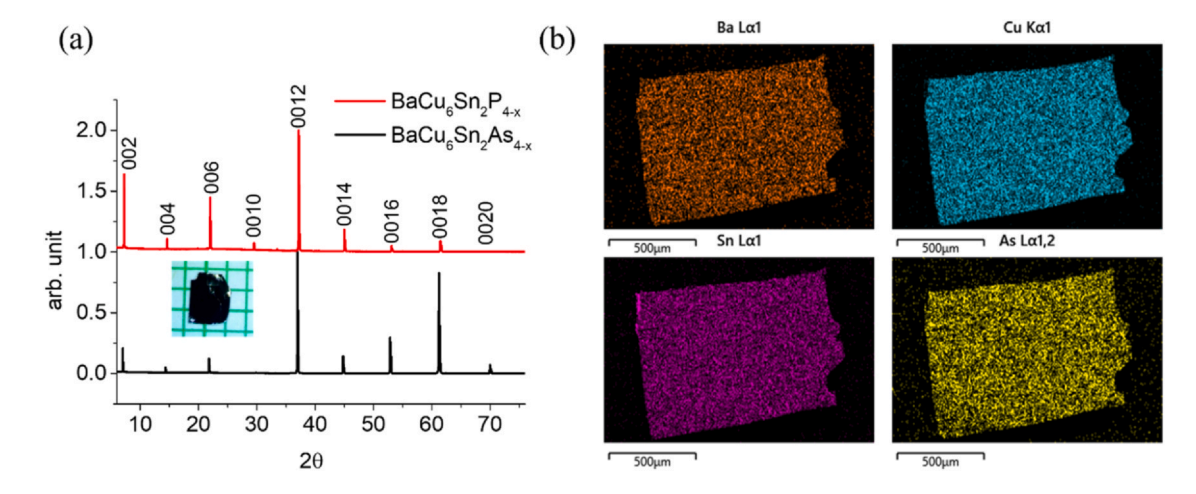


Fig. 3. (a) XRD patterns of BaCu<sub>6</sub>Sn<sub>2</sub>As<sub>2.46</sub> and BaCu<sub>6</sub>Sn<sub>2</sub>P<sub>2.72</sub> single crystals with preferred orientation along *c*-axis. Inset is optical image of BaCu<sub>6</sub>Sn<sub>2</sub>As<sub>2.46</sub> single crystal; (b) SEM-EDX mapping data for BaCu<sub>6</sub>Sn<sub>2</sub>As<sub>2.46</sub>.

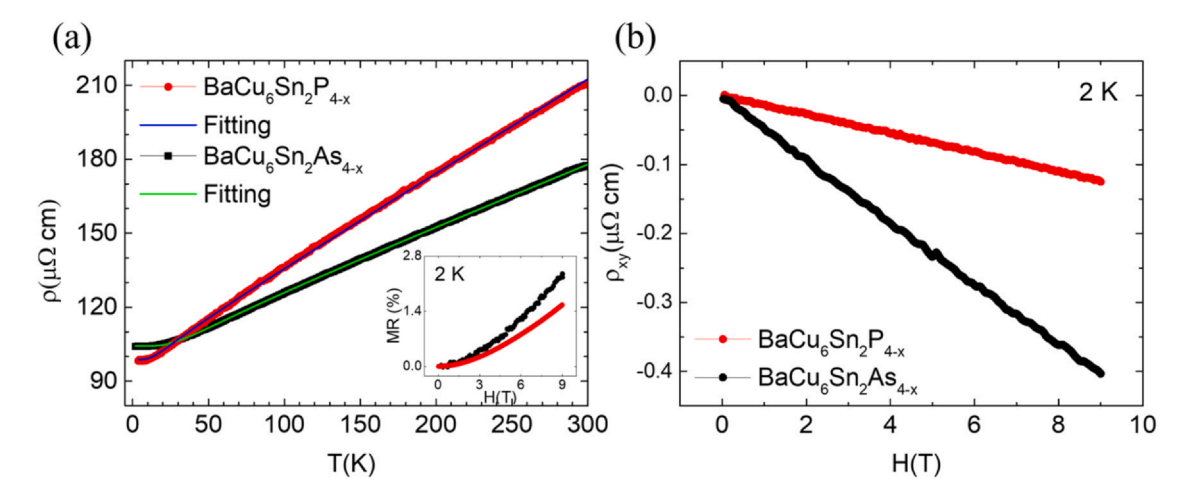


Fig. 4. (a) Temperature dependent resistivity measurement of  $BaCu_6Sn_2As_{2.46}$  and  $BaCu_6Sn_2P_{2.72}$  single crystals with fitting curves. Inset shows magnetoresistance at 2 K for  $BaCu_6Sn_2As_{2.46}$  and  $BaCu_6Sn_2P_{2.72}$  single crystals; (b) Field dependent Hall resistivity of  $BaCu_6Sn_2As_{2.46}$  and  $BaCu_6Sn_2P_{2.72}$  single crystals measured at 2 K.

cm<sup>-3</sup> for BaCu<sub>6</sub>Sn<sub>2</sub>P<sub>2.72</sub>, which are comparable with  $6.63 \times 10^{22}$  cm<sup>-3</sup> for ternary compound BaCu<sub>2</sub>As<sub>2</sub> [27].

#### 4. Conclusion

In conclusion, quaternary  $BaCu_6Sn_2As_{4-x}$  and  $BaCu_6Sn_2P_{4-x}$  phases, as the only two quaternary compounds discovered in Ba-Cu-Sn-Pn (Pn=As, P) system so far, form a new class of compounds with characteristic slab structures. The synthesis, crystal structure, and basic physical properties of the two compounds have been described. The distinct pnictogen occupancy at the tetrahedral interstitial sites formed by neighboring metal atoms with  $Cu_2Sb-type$  building motifs is rather intriguing, suggesting the possibility that this so far rather limited class of materials has great potential for discovery of a considerably larger number of compounds with similar or related packing structures. More systematical explorative synthesis and investigation on associated physical properties for these compounds would be rather interesting.

# **CRediT authorship contribution statement**

Hanlin Wu: Investigation, Formal analysis, Validation, Visualization, Writing – original draft, Preparation. Sheng Li: Formal analysis, Investigation, Writing – review & editing, Validation. Xiqu Wang: Investigation, Formal analysis. Sunah Kwon: Investigation, Formal analysis. Wenhao Liu: Investigation. Gareth A. Ofenstein: Investigation. Moon J. Kim: Resources, Investigation. Bing Lv: Conceptualization, Supervision, Resources, Writing – review & editing, Funding acquisition.

#### **Accession Codes**

CCDC 2072891, 2072892 contains the supplementary crystallographic data for this paper. These data can be obtained free of charge via <a href="www.ccdc.cam.ac.uk/data\_request/cif">www.ccdc.cam.ac.uk/data\_request/cif</a>, or by emailing data\_request@ccdc.cam.ac.uk, or by contacting The Cambridge Crystallographic Data Centre, 12 Union Road, Cambridge CB2 1EZ, UK; fax: +44 1223 336033.

### **Declaration of Competing Interest**

The authors declare that they have no known competing financial interests or personal relationships that could have appeared to influence the work reported in this paper.

#### Acknowledgments

This work at University of Texas at Dallas is supported by US Air Force Office of Scientific Research Grant No. FA9550-19-1-0037. This project is also partially funded by NSF- DMREF- 1921581, and the University of Texas at Dallas Office of Research through the Seed Program for Interdisciplinary Research (SPIRe) and Core Facility Voucher Program. M. J. K. was supported in part by the Louis Beecherl, Jr. Endowment Funds, and Global Research and Development Center Program (2018K1A4A3A01064272) and Brain Pool Program (2019H1D3A2A01061938) through the National Research Foundation of Korea (NRF) funded by the Ministry of Science and ICT.

## References

- W.B. Pearson, The Cu<sub>2</sub>Sb and related structures, Z. Krist. Cryst. Mater. 171 (1985) 23–39, https://doi.org/10.1524/zkri.1985.171.1-2.23
- [2] D.O. Charkin, X.N. Zolotova, A crystallographic re-investigation of Cu<sub>2</sub>Sb-related binary, ternary, and quaternary structures: how many structure types can exist upon the same topology of a unit cell? Crystallogr. Rev. 13 (2007) 201–245, https://doi.org/10.1080/08893110701618993
- [3] R. Pöttgen, D. Johrendt, Materials with ZrCuSiAs-type structure, Z. Naturforsch. 63b (2008) 1135–1148, https://doi.org/10.1515/znb-2008-1001
- [4] O.I. Bodak, E.I. Gladyshevskii, P.I. Kripyakevich, Crystal structure of CeFeSi and related compounds, J. Struct. Chem. 11 (1970) 283–288, https://doi.org/10.1007/ BF00745235
- [5] V. Johnson, W. Jeitschko, ZrCuSiAs: A "Filled" PbFCI Type, J. Solid State Chem. 11 (1974) 161–166. https://doi.org/10.1016/0022-4596/74/90111-X
- Y. Kamihara, T. Watanabe, M. Hirano, H. Hosono, Iron-based layered superconductor La[O<sub>1-x</sub>F<sub>x</sub>]FeAs (x = 0.05-0.12) with T<sub>c</sub> = 26 K, J. Am. Chem. Soc. 130 (2008) 3296–3297, https://doi.org/10.1021/ja800073m
  J.H. Tapp, Z. Tang, B. Lv, K. Sasmal, B. Lorenz, P.C.W. Chu, A.M. Guloy, LiFeAs: an
- [7] J.H. Tapp, Z. Tang, B. Lv, K. Sasmal, B. Lorenz, P.C.W. Chu, A.M. Guloy, LiFeAs: an intrinsic FeAs-based superconductor with T<sub>c</sub> = 18 K, Phys. Rev. B 78 (2008) 3–6, https://doi.org/10.1103/PhysRevB.78.060505
- [8] S. Borisenko, D. Evtushinsky, Q. Gibson, A. Yaresko, K. Koepernik, T. Kim, M. Ali, J. van den Brink, M. Hoesch, A. Fedorov, E. Haubold, Y. Kushnirenko, I. Soldatov, R. Schäfer, R.J. Cava, Time-reversal symmetry breaking type-II Weyl state in YbMnBi<sub>2</sub>, Nat. Commun. 10 (2019) 1–10, https://doi.org/10.1038/s41467-019-11393-5
- [9] L.M. Schoop, M.N. Ali, C. Straßer, A. Topp, A. Varykhalov, D. Marchenko, V. Duppel, S.S.P. Parkin, B.V. Lotsch, C.R. Ast, Dirac cone protected by non-symmorphic symmetry and three-dimensional Dirac line node in ZrSiS, Nat. Commun. 7 (2016) 11696, https://doi.org/10.1038/ncomms11696
- [10] P. Wadley, V. Novák, R.P. Campion, C. Rinaldi, X. Martí, H. Reichlová, J. Železný, J. Gazquez, M.A. Roldan, M. Varela, D. Khalyavin, S. Langridge, D. Kriegner, F. MácA, J. Mašek, R. Bertacco, V. Holý, A.W. Rushforth, K.W. Edmonds, B.L. Gallagher, C.T. Foxon, J. Wunderlich, T. Jungwirth, Tetragonal phase of epitaxial room-temperature antiferromagnet CuMnAs, Nat. Commun. 4 (2013) 1–6, https://doi.org/10.1038/ncomms3322
- [11] K. Yang, K. Kang, Z. Diao, A. Ramanathan, M.H. Karigerasi, D.P. Shoemaker, A. Schleife, D.G. Cahill, Magneto-optic response of the metallic antiferromagnet Fe<sub>2</sub>As to ultrafast temperature excursions, Phys. Rev. Mater. 3 (2019) 1–11, https://doi.org/10.1103/PhysRevMaterials.3.124408

- [12] S.N. Guin, Q. Xu, N. Kumar, H.H. Kung, S. Dufresne, C. Le, P. Vir, M. Michiardi, T. Pedersen, S. Gorovikov, S. Zhdanovich, K. Manna, G. Auffermann, W. Schnelle, J. Gooth, C. Shekhar, A. Damscelli, Y. Sun, C. Felser, 2D-Berry-curvature-driven large anomalous hall effect in layered topological nodal-line MnAlGe, Adv. Mater. 2006301 (2021), https://doi.org/10.1002/adma.202006301
- [13] G.R. Stewart, Superconductivity in iron compounds, Rev. Mod. Phys. 83 (2011) 1589–1652, https://doi.org/10.1103/RevModPhys.83.1589
- [14] L.M.L. Fransson, J.T. Vaughey, R. Benedek, K. Edström, J.O. Thomas, M.M. Thackeray, Phase transitions in lithiated Cu<sub>2</sub>Sb anodes for lithium batteries: an in situ X-ray diffraction study, Electrochem. Commun. 3 (2001) 317–323. https://doi.org/10.1016/S1388-2481(01)00140-0
- [15] L. Baggetto, E. Allcorn, A. Manthiram, G.M. Veith, Cu<sub>2</sub>Sb thin films as anode for Na-ion batteries, Electrochem. Commun. 27 (2013) 168–171, https://doi.org/10. 1016/i.elecom.2012.11.030
- [16] S. Ni, J. Ma, X. Lv, X. Yang, L. Zhang, The fine electrochemical performance of porous Cu<sub>3</sub>P/Cu and the high energy density of Cu<sub>3</sub>P as anode for Li-ion batteries, J. Mater. Chem. A 2 (2014) 20506–20509, https://doi.org/10.1039/c4ta03871a
- [17] K. Olejník, V. Schuler, X. Marti, V. Novák, Z. Kašpar, P. Wadley, R.P. Campion, K.W. Edmonds, B.L. Gallagher, J. Garces, M. Baumgartner, P. Gambardella, T. Jungwirth, Antiferromagnetic CuMnAs multi-level memory cell with microelectronic compatibility, Nat. Commun. 8 (2017) 15434, https://doi.org/10.1038/pcomps.15434
- [18] A. Mewis, Darstellung und Struktur der Verbindungen MgCuP, BaCuP(As) und BaAgP(As)/Preparation and Crystal Structure of MgCuP BaCuP(As), and BaAgP (As), Z. Nat. 34b (1979) 1373–1376, https://doi.org/10.1515/znb-1979-1006
- [19] M. Pfisterer, G. Nagorsen, Zur Struktur ternärer Übergangsmetallarsenide/On the Structure of Ternary Arsenides, Z. Naturforsch. 35b (1980) 703–704, https://doi. org/10.1515/znb-1980-0611
- [20] J. Dünner, A. Mewis, Synthese und Kristallstruktur von ACu<sub>4</sub>As<sub>2</sub> (A: Ca-Ba, Eu) /Synthesis and Crystal Structure of ACu<sub>4</sub>As<sub>2</sub> (A: Ca-Ba, Eu), Z. Anorg. Allg. Chem. 625 (1999) 625-628, https://doi.org/10.1002/(SICI)1521-3749(199904) 625:4-625::AID-ZAAC625-3.0.CO:2-Z
- [21] J. Dünner, A. Mewis, BaCu<sub>6</sub>P<sub>2</sub> and BaCu<sub>6</sub>As<sub>2</sub> two compounds with a periodic intergrowth of ThCr<sub>2</sub>Si<sub>2</sub> and Cu structure-type segments, J. Alloys Compd. 221 (1995) 65–69, https://doi.org/10.1016/0925-8388(94)01431-0
- [22] İ. Pilchowski, A. Mewis, M. Wenzel, R. Gruehn, BaCu<sub>8</sub>P<sub>4</sub> und BaCu<sub>8</sub>As<sub>4</sub>: Darstellung, Strukturbestimmung und elektronenmikroskopische Untersuchungen, Z. Anorg. Allg. Chem. 588 (1990) 109–116, https://doi.org/10. 1002/zaac.19905880114
- [23] J. Dünner, A. Mewis, M. Roepke, G. Michels, Neue ternare Kupferpnictide rnit modifizierten BaAl<sub>4</sub>-Strukturen/New Ternary Copper Pnictides with Modified BaAl<sub>4</sub>-Type Structures, Z. Anorg. Allg. Chem. 621 (1995) 1523–1530, https://doi. org/10.1002/zaac.19956210915
- [24] A. Mewis, Ternäre Phosphide mit ThCr<sub>2</sub>Si<sub>2</sub>- Struktur/Ternary Phosphides with the ThCr<sub>2</sub>Si<sub>2</sub> Structure, Z. Nat. 35b (1980) 141–145, https://doi.org/10.1515/znb-1980.0205

- [25] V.G. Cordier, B. Eisenmann, H. Schäfer, Darstellung und Kristallstruktur von SrCu<sub>2</sub>Sb<sub>2</sub> und SrZnBi<sub>2</sub>, Z. Anorg. Allg. Chem. 426 (1976) 205–214, https://doi.org/ 10.1002/zaac.19764260210
- [26] V.K. Anand, P.K. Perera, A. Pandey, R.J. Goetsch, A. Kreyssig, D.C. Johnston, Crystal growth and physical properties of SrCu<sub>2</sub>As<sub>2</sub>, SrCu<sub>2</sub>Sb<sub>2</sub>, and BaCu<sub>2</sub>Sb<sub>2</sub>, Phys. Rev. B 85 (2012) 1–24. https://doi.org/10.1103/PhysRevB.85.214523
- [27] H. Wu, S. Li, Z. Wu, X. Wang, G.A. Ofenstein, S. Kwon, M.J. Kim, P.C.W. Chu, B. Lv, Novel polymorphic phase of BaCu<sub>2</sub>As<sub>2</sub>: impact of flux for new phase formation in crystal growth, Cryst. Growth Des. 20 (2020) 5922–5930, https://doi.org/10. 1021/acs.cgd.0c00614
- [28] L. Krause, R. Herbst-Irmer, G.M. Sheldrick, D. Stalke, Comparison of silver and molybdenum microfocus X-ray sources for single-crystal structure determination, J. Appl. Crystallogr. 48 (2015) 3–10, https://doi.org/10.1107/S1600576714022985
- [29] G.M. Sheldrick, Crystal structure refinement with SHELXL, Acta Crystallogr. Sect. C Struct. Chem. 71 (2015) 3–8, https://doi.org/10.1107/S2053229614024218
- [30] H. Knödler, Der strukturelle Zusammenhang zwischen γ- und ε-Phase im System Kupfer-Zinn, Acta Crystallogr. 10 (1957) 86–87, https://doi.org/10.1107/ s0365110×57000225
- [31] S. Lidin, A.-K. Larsson, A Survey of Superstructures in Intermetallic NiAs-Ni<sub>2</sub>In-Type Phases, J. Solid State Chem. 118 (1995) 313–322, https://doi.org/10.1006/ issc.1995.1350
- [32] W. Dörrscheidt, G. Savelsberg, J. Stöhr, H. Schäfer, Beiträge zu den stabilitätskriterien der BaCuSn<sub>2</sub>-struktur: Die verbindungen LaCu<sub>0.5e</sub>Sn<sub>2</sub>, LaNi<sub>0.74</sub>Sn<sub>2</sub>, LaCo<sub>0.52</sub>Sn<sub>2</sub>, LaFe<sub>0.34</sub>Sn<sub>2</sub> und BaCuSn<sub>2</sub>, J. Less Common Met. 83 (1982) 269–278, https://doi.org/10.1016/0022-5088(82)90277-6
- [33] R. Pöttgen, G. Kotzyba, Structure refinement and magnetic properties of DyCuSn, J. Alloys Compd. 245 (1996) 7–10, https://doi.org/10.1016/S0925-8388(96) 02398-5
- [34] B. Eisenmann, H. Jordan, H. Schäfer, Phasen im Grenzbereich der Zintlkonzeption: Zur Kenntnis von Sr<sub>5</sub>Sn<sub>2</sub>P<sub>6</sub> und SrSnP, J. Less Common Met. 116 (1986) 251–258, https://doi.org/10.1016/0022-5088(86)90233-X
- [35] B. Eisenmann, H. Jordan, H. Schäfer, Ba<sub>3</sub>Sn<sub>2</sub>P<sub>4</sub>, ein neues Inophosphidostannat (III), Z. Anorg. Allg. Chem. 532 (1986) 73–80, https://doi.org/10.1002/zaac. 19865320112
- [36] B. Eisenmann, H. Jordan, H. Schäfer, Ca<sub>5</sub>Sn<sub>2</sub>As<sub>6</sub>, das erste Inoarsenidostannat(IV), Z. Anorg. Allg. Chem. 530 (1985) 74–78, https://doi.org/10.1002/zaac. 19855301108
- [37] B. Eisenmann, H. Jordan, H. Schäfer, Ba<sub>3</sub>Sn<sub>2</sub>As<sub>4</sub>, eine neue Zintlphase mit Kettenstruktur/ On Ba<sub>3</sub>Sn<sub>2</sub>As<sub>4</sub>, a New Zintl Phase with Chain Structure, Z. Naturforsch. 39b (1984) 1151–1153, https://doi.org/10.1515/znb-1984-0828
- [38] W.L. Chiu, C.M. Liu, Y.S. Haung, C. Chen, Formation of nearly void-free Cu<sub>3</sub>Sn intermetallic joints using nanotwinned Cu metallization, Appl. Phys. Lett. 104 (2014) 171902. https://doi.org/10.1063/1.4874608
- [39] W.B. Pearson, Electrical resistivity, hall coefficient, and thermoelectric power of AuSb<sub>2</sub> and Cu<sub>2</sub>Sb, Can. J. Phys. 42 (1964) 519–525, https://doi.org/10.1139/p64-047